TERAHERTZ BAND FREE ELECTRON LASERS WITH HYBRID BRAGG REFLECTORS*

N. Ginzburg, A. Malkin#, N. Peskov, A. Sergeev, V. Zaslavsky, IAP RAS, Nizhny Novgorod, Russia

Abstract

Periodical Bragg structures can be considered as an effective way of controlling the electromagnetic energy fluxes and provision of spatial coherence of radiation in the electron devices with oversized interaction space. Advance of long-pulse FEL with 2D distributed feedback into the terahertz waveband can be achieved by using a two-mirror scheme in which an advanced Bragg reflector (a periodical structure exploiting the coupling between the two counter-propagating waves and a cutoff mode) is used as an upstream mirror. In the planar model considered in the present paper this reflector provides effective mode selection over the "narrow" transverse coordinate directed between the plates. Synchronization of radiation from a sheet electron beam over the "wide" coordinate can be obtained by exploiting structures providing 2D distributed feedback used as a downstream mirror.

INTRODUCTION

Distributed feedback (DFB) involving periodical Bragg structures is widely used in generators of coherent radiation based on principles of both classical and quantum electronics. Correspondingly the frequency range in which the oscillators of this type function includes millimeter and optical (infrared) bands [1-4]. In the present work we show that Bragg structures of a specific type can be effectively used in application in the Terahertz range in application to free electron lasers (FEL). The advantage of suggested structures along with their compatibility with intense electron beam transport systems is the possibility of mode selection over both transverse and longitudinal indices which is a necessary condition of obtaining the spatially coherent radiation in oversized electrodynamical systems.

The planar scheme of THz band FEL under consideration is shown in Fig.1. We suggest using a hybrid two-mirror cavity as an electrodynamical system consisting of an advanced Bragg structure as an input mirror and a conventional Bragg reflector as an output mirror. Bragg structures (reflectors) are formed by the sections of a planar waveguide with shallow sine corrugation of the surface

$$b(z) = b_0 + b_j \cos(\bar{h}_j z), \qquad (1)$$

where b_0 is the gap between the plates, b_j are the amplitudes of corrugation, $\bar{h}_j = 2\pi/d_j$, d_j are their periods. Here index $j = 1$ refers to the parameters of the input structure and the index $j = 2$ to the parameters of the output one.

In a conventional output Bragg reflector the coupling between the two paraxial wave beams propagating in opposite directions is employed when the Bragg resonance condition is satisfied

$$\bar{h}_2 \approx 2h, \qquad (2)$$

where h is the longitudinal wavenumber of both forward and backward waves. The peculiarity of the advanced Bragg reflector scheme is the use of coupling between the longitudinal and transverse (with respect to the direction of the particles translational velocity $\vec{V} = \vec{z}_0 V_0$) wave beams when the following Bragg resonance condition is satisfied

$$\bar{h}_1 \approx h. \qquad (3)$$

Obviously the period of the advanced Bragg mirror is two times larger than the one of the conventional Bragg structure. Reflections into the wave beams propagating in the transverse directions (along the y axis, see Fig.1) forming the standing wave (the cutoff mode) take place when the gap between the plates and the corrugation period are bound by the following condition:

$$b_0 \approx sd_1/2, \qquad (4)$$

where s is integer. Within the regular planar waveguide

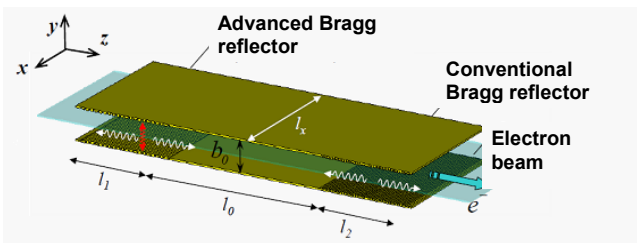

Figure 1: The scheme of planar FEL with advanced input and conventional output Bragg reflectors.

mode classification the described wave beams form the TM_s mode with its frequency close to the cutoff one $\omega_c = \pi sc/b_0$.

In the present paper we investigate the dynamics of FEL with the `described type of a hybrid Bragg cavity. Unlike the previous works [5,6] the transverse structure of paraxial wave beams is not assumed to be fixed which allows us to be more accurate in determining the maximum acceptable oversize factor (ratio between the gap b_0 and the wavelength λ) that allows to maintain the coherence of radiation, which leads in fact to the frequency range of the suggested FEL scheme.

We also show that by combining the advanced Bragg mirror with two-dimensional one the spatial coherence of

*Work supported by RFBR grant 08-08-00966
#malkin@appl.sci-nnov.ru

the output radiation can be obtained over both transverse coordinates.

THE MODEL AND BASIC EQUATIONS

First we consider a 2D model assuming that the planar waveguide is infinite along the "wide" transverse coordinate (x in Fig.1). When the Bragg scattering condition (3) is satisfied the field in the advanced Bragg structure can be can be presented as a sum of the two quasi-optical *TM* type beams propagating in opposite directions

$$\vec{H} = \vec{x}_0 \,\mathrm{Re}\left[a_+(z,y,t)e^{i(\omega t - hz)} + a_-(z,y,t)e^{i(\omega t + hz)}\right] \qquad (5a)$$

and a cutoff TM_S mode

$$\vec{H} = \vec{x}_0 \,\mathrm{Re}\left[f(z,t)\sin(h_\perp y)e^{i\omega t}\right]. \qquad (5b)$$

Here $a_\pm(z,y,t)$ and $f(z,t)$ are slowly varying in time and space and the carrier frequency is chosen to be equal to the cutoff frequency $\omega = \omega_c$.

In an FEL the electron flow wiggling in the undulator field interacts with and amplifies the co-moving wave beam a_+ in the conditions of the combination synchronism

$$\omega - hV_0 \approx h_u V_0, \qquad (6)$$

where $h_u = 2\pi/d_u$ and d_u is the wiggler field period. The synchronous wave a_+ scatters into the backward wave a_- via the excitation of the cutoff mode f on a Bragg structure (1). As a result the coupling between the cutoff and propagating wave beams makes it possible to combine the mode selection mechanisms used in gyrotrons and orotrons ([7] and [8]) with frequency Doppler up-conversion typical for FEL.

Non-stationary equations for the amplitudes of coupled waves can be presented in the form

$$\begin{aligned}
&\frac{\partial \hat{a}_+}{\partial Z} + \frac{\partial \hat{a}_+}{\partial \tau} + i\frac{\partial^2 \hat{a}_+}{\partial Y^2} + \sigma \hat{a}_+ = \\
&\qquad = i\frac{\alpha_1 B}{2}\hat{f}\left[\delta(Y) + \delta(Y-B)\right] + F(Y)J \\
&-\frac{\partial \hat{a}_-}{\partial Z} + \frac{\partial \hat{a}_-}{\partial \tau} + i\frac{\partial^2 \hat{a}_-}{\partial Y^2} + \sigma \hat{a}_- = \\
&\qquad = i\frac{\alpha_1 B}{2}\hat{f}\left[\delta(Y) + \delta(Y-B)\right] \\
&\frac{\partial \hat{f}}{\partial \tau} + \frac{iC}{2}\frac{\partial^2 \hat{f}}{\partial Z^2} + \sigma \hat{f} = \\
&\qquad = i\alpha_1\left[(\hat{a}_+ + \hat{a}_-)\big|_{Y=0} + (\hat{a}_+ + \hat{a}_-)\big|_{Y=B}\right],
\end{aligned} \qquad (7)$$

where $\delta(Y)$ is the delta function. Here we used the following normalized variables and parameters

$$Z = C\frac{\omega_c}{c}z, \quad Y = \sqrt{2C}\frac{\omega_c}{c}y, \quad \tau = C\omega_c t, \quad \hat{a}_\pm = \frac{e\mu K a_\pm}{2mc\omega_c\gamma_0^2 C^2}, \quad ,$$

$\hat{f} = \dfrac{e\mu K f}{2\sqrt{2}mc\omega_c\gamma_0^2 C^2}$, $C = \left(\dfrac{eI_0\mu K^2\lambda^2}{8\pi mc^3\gamma_0^3 b_0}\right)^{1/3}$ is the Pierce parameter, I_0 is the beam current density, $K = eH_u/h_u mc^2$, H_u is the undulator field amplitude, $\mu \approx \gamma_0^{-2}\left(1+K^2\right)$ is the electorns' inertial bunching parameter, $\gamma_0 = \left(1-\beta_0^2\right)^{-1/2}$, $\lambda = 2\pi c/\omega_c$, $\sigma = \dfrac{h\nu}{b_0}$ is the Ohmic losses parameter for the cutoff mode, ν is the skin depth (Ohmic losses for propagating waves $A_\pm$ are negligibly small), $\alpha_1 = b_1/Cb_0\sqrt{2}$ is the waves coupling coefficient, $F(Y)$ describes the transverse distribution of the electron current. The excitation factor for the synchronous wave, the RF current

$$J = 1/\pi\int_0^{2\pi} e^{-i\theta}d\theta_0$$

can be found from the averaged particles' motion equations

$$\left(\frac{\partial}{\partial\tau} + \beta_0^{-1}\frac{\partial}{\partial Z}\right)^2\theta = Re\left(\hat{a}_+ e^{i\theta}\right) \qquad (8)$$

with boundary conditions

$$\theta\big|_{Z=0} = \theta_0 \in [0,2\pi), \quad \left(\partial/\partial\tau + \beta_0^{-1}\,\partial/\partial Z\right)\theta\Big|_{Z=0} = -\Delta. \qquad (9)$$

In the conventional output Bragg mirror the direct coupling between forward and backward propagating wave beams takes place which can be described by the equations

$$\begin{aligned}
&\frac{\partial \hat{a}_+}{\partial Z} + \frac{\partial \hat{a}_+}{\partial \tau} + i\frac{\partial^2 \hat{a}_+}{\partial Y^2} + \sigma \hat{a}_+ = \\
&\qquad = i\frac{\alpha_2 B}{2}\hat{a}_-\left[\delta(Y) + \delta(Y-B)\right] + F(Y)J \\
&-\frac{\partial \hat{a}_-}{\partial Z} + \frac{\partial \hat{a}_-}{\partial \tau} + i\frac{\partial^2 \hat{a}_-}{\partial Y^2} + \sigma \hat{a}_- = \\
&\qquad = i\frac{\alpha_2 B}{2}\hat{a}_-\left[\delta(Y) + \delta(Y-B)\right],
\end{aligned} \qquad (10)$$

where $\alpha_2 = b_2/Cb_0\sqrt{2}$.

In the regular resonator section we describe the dynamics of electron-wave interaction by the Eqs. (7) or (10) where we put $\alpha_1 = \alpha_2 = 0$.

For propagating waves boundary conditions at resonator edges take a form

$$\hat{A}_+\big|_{Z=0} = \hat{A}_0, \quad \hat{A}_-\big|_{Z=L} = 0, \qquad (11)$$

For the cutoff mode we apply the radiation boundary conditions at the edges of corrugation [9,10]

$$\left[\hat{B} \mp \sqrt{\frac{C}{2\pi i}}\int_0^\tau \frac{e^{-\bar{\sigma}(\tau-\tau')-iS(\tau-\tau')}}{\sqrt{\tau-\tau'}}\frac{\partial\hat{B}(\tau')}{\partial Z}d\tau'\right]_{Z=0,L} = 0, \qquad (12)$$

where L is the normalized length of the resonator $L=Chl$.

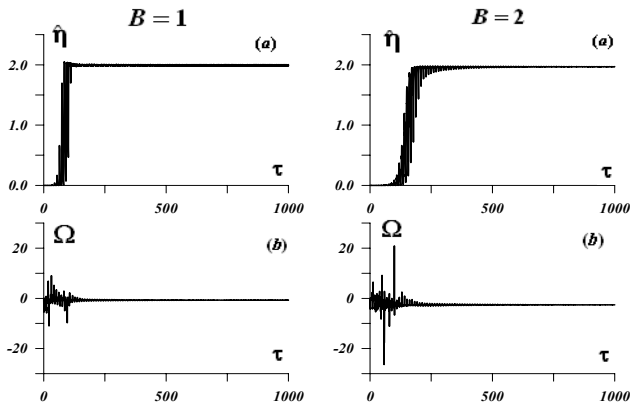

Figure 2: Establishment of steady state oscillations at various values of the gap parameter B. Here the efficiency (up) and the normalized radiation frequency (down) temporal dependencies are depicted.

Electron efficiency is determined by the following relations

$$\eta = \frac{C}{\mu\left(1-\gamma_0^{-1}\right)}\bar{\eta}$$
$$\bar{\eta} = \frac{1}{2\pi b_0}\int_0^{b_0}\int_0^{2\pi}\left(\frac{\partial\theta}{\partial Z}-\Delta\right)\Big|_{Z=L} d\theta_0 dY \qquad (13)$$

SIMULATIONS AND RESULTS

Eqs (7-10). were simulated using the multiwave approach that consists in expanding the field into the series of transverse waveguide modes (see [11]).

We simulate the nonlinear dynamics of an FEL for the working frequency f=1 THz. We took the particles energy to be 5.5 MeV, the undulator period 4 cm, and the undulator field amplitude H_u=2.8 kOe. In this case for a sheet electron beam with injection current density 130 A/cm^2 the Pierce parameter is $C \approx 1.4\cdot 10^{-4}$. Lengths of the input and the output Bragg reflectors were taken $l_{1,2}$=13.5 cm, corrugation depths $2b_1 = 5$ μm and $2b_2 = 1.5$ μm, and the periods $d_1 = 0.03$ cm and $d_2 = 0.015$ cm; the length of regular section was taken l_0=150 cm.

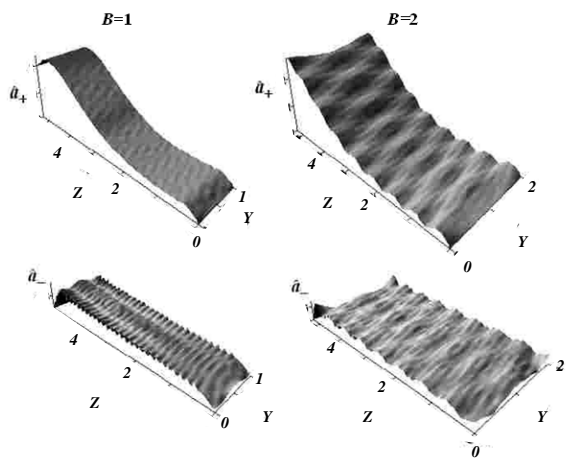

Figure 3: Spatial structures of the partial waves in the steady-state regime.

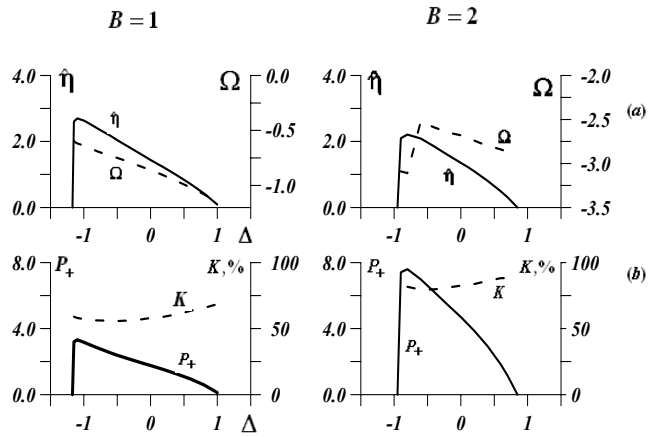

Figure 4: Dependence of the steady state regime characteristics on the frequency synchronism detuning.

In Fig.2 we present the results of simulation of the steady-state oscillation regime establishment. Spatial distributions of the partial waves fields $\hat{a}_{\pm}$ in the steady-state regime presented in Fig.3 show that at the gap values reaching 20λ the output radiation possess rather high spatial homogeneity and its structure is close to the *TEM* mode.

Simulation shows that at the chosen oversize factor the input advanced Bragg reflector provides the establishment of single-frequency steady-state regime (Fig.2). This regime is stable to the changing of electron beam parameters. In Fig.4 we show that varying the electron synchronism mismatch Δ parameter leads to the smooth changing of the radiation frequency. At $B = 1$ there are no frequency jumps and at $B = 2$ there is a single frequency jump near the boundary of the oscillations band.

Thus the suggested scheme of THz band FEL allows to provide the conditions of self-excitation, effective energy extraction and spatial coherence of radiation at the

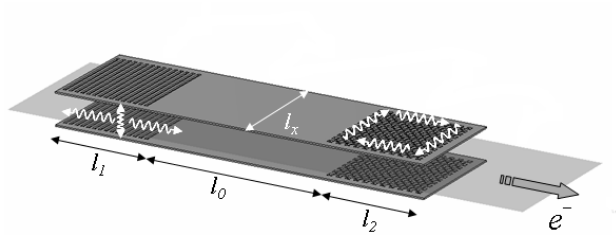

Figure 5: The scheme of planar FEL with advanced input and 2D output Bragg reflectors.

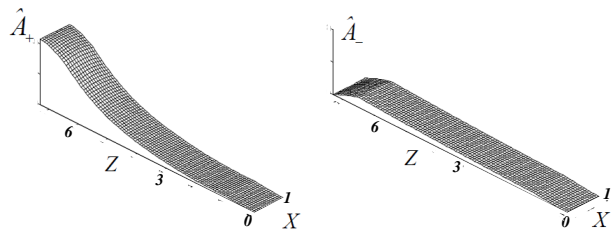

Figure 6. Spatial structures of the propagating waves excited in an FEL with advanced Bragg and 2D Bragg reflectors.

oversize factors not less than 10-20 wavelengths which is sufficient for the forming of transportation channel for the intense sheet beam. Simulation shows that at $b_0 = 20\lambda$ up to 80% of radiated power is carried from the interaction space with forward wave $\hat{a}_+$. At the electron efficiency of $\eta \sim 2\%$ power density is about 6.5 MW/cm. Time of oscillations' establishment reaches 300 ns.

It is important to note that for a planar system open in the $\vec{x}$ direction (see Fig.1), the spatial synchronization along this coordinate should be provided by the diffraction of radiation while the corresponding Fresnel parameter

$$N_F = l_x^2 / l_{eff}\lambda \le 1,$$

где $l_{eff} = l_0/(1 - R_1R_2)$ is the effective length of propagation that takes into account the finite values of

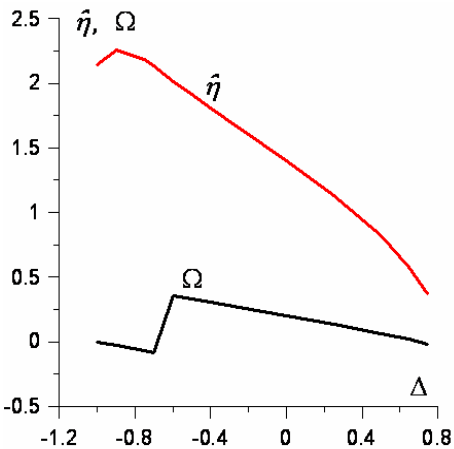

Figure 7: Dependence of radiation frequency and the efficiency on electron synchronism mismatch.

mirrors' reflection coefficients $R_{1,2}$. At the chosen parameters the allowable width of the oscillator l_x is in the order of several centimeters which is comparable to the dimensions of FEL with conventional quasi-optical cavities [12-14].

For the width of the system exceeding the stated limits the transverse synchronization of radiation can be obtained by using the 2D distributed feedback Bragg structure [15] used as a downstream mirror. This system is depicted in Fig.5. Fig.6 shows the spatial structures of the excited fields are shown evidencing the synchronization of radiation over the x coordinate. Fig.7 shows the dependence of radiation frequency on electron synchronism mismatch illustrating the stability of radiation frequency to the varying beam parameters. Estimations in this case that for the current of 120 A/cm and electrons energy of 6.5 MeV the 1 THz oscillation regime can be realized with the output power of 350 MW at the efficiency of 2%.

REFERENCES

[1] H. Kogelnik, C.V. Shank, J. Appl. Phys, 1972, vol. 43 pp. 2327-2335.
[2] A. Yariv, Quantum Electronics, Wiley, 1975
[3] N.S. Ginzburg, V.L. Bratman, G.G. Denisov, M.I. Petelin, IEEE J. of Quant. Electr., 1983, vol.QE-19, no.3, pp.282-298.
[4] N.S. Ginzburg, A.A. Kaminsky, A.. Kaminsky, et al., Phys. Rev. Lett., 2000, vol.84, pp.3574-3577.
[5] N.S. Ginzburg, A.M. Malkin, A.A. Kaminsky, et al., Phys. Rev. ST–AB,2005, vol. 8, 040705.
[6] N S. Ginzburg, A. M. Malkin, N. Yu. Peskov, et al., Phys. Rev. ST–AB, 2009, 12, 060702.
[7] A.V. Gaponov, A.L. Goldenberg, D.P. Grigoriev, et al., ZhETP Letters, 1965, V.2, N.9, P. 430 [in Russian].
[8] F.S. Rusin, G.D. Bogomolov, ZhETP Letters, 1966, V.4, N.6, P. 236 [in Russian]
[9] N.S. Ginzburg, N.A. Zavolsky, G.S. Nusinovich, A.S. Sergeev, Sov. Radiophys. Quantum Electron., 1986, 29, pp. 89–97.
[10] N.S. Ginzburg, G.S. Nusinovich and N.A. Zavolsky, Int. J. Electronics, 1986, vol. 61, p. 881.
[11] N. S. Ginzburg, V.Yu. Zaslavsky, I.V. Zotova, A.M. Malkin, N.Yu. Peskov, A.S. Sergeev, JETP Letters, 2010, Vol. 91, No.6, P. 266.
[12] Dem'yanenko M.A., Esaev D.G., Knyazev B.A., et al., Appl. Phys. Lett. 2008. V.92. P.131116.
[13] Neil G.R., Bohn C.L., Benson S.V., et al., Phys. Rev. Lett. 2000. V.84. P.662.
[14] Kazakevich G.M., Pavlov V.M., Jeong Y.U., et al., Phys. Rev.ST-AB. 2009. V.12. P.040701.
[15] N.S. Ginzburg, N.Yu. Peskov, A.S. Sergeev, et al., JETP Letters, 2010, to be published.